β decay of ^{100}In

C. Plettner,[1,2] L. Batist,[3] J. Döring,[1] A. Blazhev,[1,4] H. Grawe,[1] V. Belleguic,[5] C.R. Bingham,[6] R. Borcea,[1] M. Gierlik,[7] M. Górska,[1] N. Harrington,[8] Z. Janas,[7] M. Karny,[7] R. Kirchner,[1] C. Mazzocchi,[1,9] P. Munro,[8] E. Roeckl,[1] K. Schmidt,[8] and R. Schwengner[10]

[1]*Gesellschaft für Schwerionenforschung, D-64291 Darmstadt, Germany*
[2]*National Institute for Nuclear Physics and Engineering, Bucharest RO-76900, Romania*
[3]*St. Petersburg Nuclear Physics Institute, RU-188-350 Gatchina, Russia*
[4]*University of Sofia, BG-1164 Sofia, Bulgaria*
[5]*Université de Paris Sud, F-91405 Orsay, France*
[6]*Department of Physics and Astronomy, University of Tennessee, Knoxville, Tennessee 37996*
[7]*Institute of Experimental Physics, University of Warsaw, PL-00681 Warsaw, Poland*
[8]*University of Edinburgh, Edinburgh EH9 3JZ, United Kingdom*
[9]*Universitá degli Studi di Milano, I-20133 Milano, Italy*
[10]*Institut für Kern- und Hadronenphysik, FZ Rossendorf, D-01314 Dresden, Germany*
(Received 30 July 2002; published 30 October 2002)

The β decay of ^{100}In, the one proton hole and one neutron particle neighbor to ^{100}Sn, was investigated at the GSI on-line mass separator by using germanium detectors and a NaI total-absorption spectrometer. On the basis of $\beta\gamma\gamma$ coincidences, the ^{100}In decay scheme was established for the first time. The ground-state spin and parity for ^{100}In are discussed by investigating β feeding of levels in ^{100}Cd and β-delayed proton emission to ^{99}Ag. The half-life was remeasured and found to be 5.9(2) s. The Q_{EC} value was determined from the measured EC/β^+ ratio for the β-delayed protons to be 10.08(23) MeV. The main fraction of the β feeding was established to populate the region of 6 MeV excitation energy, which corresponds to a total Gamow-Teller (GT) strength of 3.9(9) and a centroid at 6.4 MeV. Large-scale shell-model calculations employing a realistic interaction are used to assign configurations to states in ^{100}In and ^{100}Cd. The GT β-decay strength distribution measured in the total absorption experiment is compared to shell-model predictions. The deduced overall hindrance of the GT strength agrees with the values predicted for the ^{100}Sn GT decay.

I. INTRODUCTION

Beta decay and in-beam investigations following fusion-evaporation reactions provide the adequate tools for exploring the structure of nuclei near the double shell closure at $N=Z=50$. The main topics of interest which characterize this mass region are single-particle energies and shell gaps as determined by the nuclear mean field, residual interaction—specifically in the proton-neutron ($\pi\nu$) channel—and the Gamow-Teller (GT) strength of the $\pi g_{9/2}\rightarrow \nu g_{7/2}$ transition. ^{100}In, representing the $\pi\nu$ particle-hole (ph) configuration with respect to the doubly magic nucleus ^{100}Sn, is the closest-lying neighbor to this core nucleus which is accessible to detailed $\beta\gamma\gamma$ spectroscopy while still having a simple ph shell-model structure. Due to the attractive $(\sigma\cdot\sigma)(\tau\cdot\tau)$ part of the nucleon-nucleon interaction, which is strongest in $\pi\nu$ pairs of spin-flip partners, e.g., $\pi g_{9/2}\nu g_{7/2}$ [1], the $\nu d_{5/2}-\nu g_{7/2}$ spacing decreases with filling of the $\pi g_{9/2}$ orbital towards ^{100}Sn [2]. Therefore the ph multiplets $[\pi g_{9/2}^{-1}\nu d_{5/2}]_{2-7}$ and $[\pi g_{9/2}^{-1}\nu g_{7/2}]_{1-8}$ provide the leading configurations which determine the ground-state spin of ^{100}In. Values of 6^+ and 7^+, respectively, are expected to become the lowest-lying members of these multiplets. Their centroids are predicted to be very close in energy [3,4].

Under the assumption that the ground state of ^{100}In has a spin of 6 or 7, the GT decay of a $g_{9/2}$ proton to a $g_{7/2}$ neutron in ^{100}Cd will preferably populate either the $J^{\pi}=(5-7)^+$

members of the two-quasiparticle ($2qp$) configurations $\nu d_{5/2}g_{7/2}$ or $\nu g_{7/2}^2$ at low excitation energy, or the $4qp$ configurations in the GT resonance [5]. In the latter case, the neutron orbitals are coupled to an unpaired $\pi g_{9/2}^{-2}$ state, with GT transitions selecting spins between 5 and 8. The low-lying members of the $2qp$ multiplet occur well below the GT resonance in a region of low level density, and their GT feeding and γ deexcitation may thus be used to assign configurations to parent and daughter states. These ^{100}Cd states have simple configurations which are easily accessible to shell-model interpretation [6–8]. In the $N=51$ isotones ^{96}Rh and ^{98}Ag, a ground state with $J^{\pi}=6^+$ has been found [9,10], and the same was adopted for the ground states of ^{102,104}In in recent in-beam and decay studies [11–13]. In contrast to that, evidence for a $J^{\pi}=7^+$ assignment for the ^{102}In ground state was inferred from the study of ^{102}Sn β decay [14]. In ^{104}In a low-lying isomer was found, with a half-life of 15.7 s and a tentative spin and parity assignment of (3^+) [15].

On the basis of the aforementioned arguments, it is decisive for the verification of the $\pi\nu$ residual interaction to experimentally determine the spin of the ground state of ^{100}In. The decay of ^{100}In has been previously investigated by measuring positrons and β-delayed protons (βp) from mass-separated sources, yielding a half-life of 6.1(9) s [12]. Recently, in a study of ^{100}In following a fragmentation reaction, a half-life of 6.6(7) s was obtained [14].

In the present report, the following topics are addressed: (i) spin-parity and configuration assignments to the ^{100}In ground state, (ii) search for a possible β-decaying isomer of ^{100}In, (iii) experimental level scheme of the daughter nucleus ^{100}Cd completing the nonyrast $J^{\pi}=(5-8)^+$ part of the scheme, (iv) experimental GT distribution, and (v) comparison of the experimental data to large-scale shell-model calculations. These items have been addressed by employing a high-resolution (composite Ge detectors) setup and a total-absorption spectrometer (TAS). Preliminary results from this work were communicated in several conference contributions [16,17].

II. EXPERIMENTAL TECHNIQUES

A. Production and mass separation

^{100}In was produced via the ^{50}Cr(^{58}Ni,$\alpha p3n$) reaction. A ^{58}Ni beam of 6.20 MeV/nucleon was delivered by the UNILAC accelerator of GSI Darmstadt. The beam impinged on a 96.9% enriched ^{50}Cr target of 3.5 mg/cm^2 thickness, backed by a molybdenum foil of 2 mg/cm^2 thickness. The reaction recoils were stopped inside a catcher of a thermal ion source [18]. The suppression of the isobaric silver and cadmium contaminants was achieved by making use of the differences in their ionization potentials with respect to that of the indium isotope. After ionization and extraction from the ion source, the beam delivered by the GSI mass separator was directed to the high-resolution or to the total-absorption setup.

B. High-resolution experiment

The $A=100$ beam was implanted into a tape during 16 s, with the tape being moved at the end of this interval. The total number of tape cycles amounted to 18 600, which corresponds to a measuring time of 83 h. The implantation point was surrounded by a plastic scintillator of 70% efficiency used to detect positrons. Gamma-ray detection was achieved by means of a hyperpure germanium detector (HPGe), an EUROBALL-type cluster [19], a superclover from the VEGA array [20] complemented by a low-energy photon spectrometer (LEPS). The high-resolution $\beta\gamma\gamma$ setup was similar to that used in a previous experiment [21]. Energy and time events from the individual Ge detectors and from the plastic scintillator were taken, digitized, and written in list mode on magnetic tape. A γ-energy range up to 4 MeV was utilized. For the time events, time-to-digital converters with time ranges of 1 μs for the cluster and 400 ns for the other Ge detectors were used. The accumulation of events was triggered by a logic "*OR*" condition of the timing signals originating from: γ singles, $\beta\gamma$, and $\gamma\gamma$ events. In case of an accepted event, a signal gate of 8 μs length was generated and applied to all analog-to-digital converters.

Energy and efficiency calibrations for each of the 13 individual Ge detectors together with the gain matching were performed off-line. Standard γ-ray sources of ^{133}Ba and ^{152}Eu were used for this purpose, covering an energy range from 30 to 1408 keV. The photopeak γ-detection efficiency for the Ge array amounted to 2.7(1)% at 1.33 MeV γ-ray

TABLE I. Level energies (E_x), spins and parities of the initial states (J^{π}), energies of the deexciting transitions (E_{γ}), and relative intensities (I_{γ}) of the γ rays normalized to the $2^+\rightarrow0^+$ transition. The J^{π} assignments are based on the β-decay results from this work and on in-beam data from Refs. [6,7].

E_x (keV)	J^{π} ($\hbar$)	E_{γ} (keV)	I_{γ} (%)
1004.1(1)	2^+	1004.1(1)	100(5)
1799.0(1)	4^+	794.9(1)	88(5)
2046.0(2)	4^+	1041.9(2)	8.1(6)
2095.8(1)	6^+	296.8(1)	60(3)
2457.7(4)	6^+	362.7(1)	8.9(10)
		411.7(3)	2.8(4)
		658.2(3)	4.2(4)
2548.6(1)	8^+	452.8(1)	9.4(8)
3164.3(1)	$(5^-, 6^+)$	1068.5(2)	2.9(4)
		1365.3(5)	2.5(5)
3199.8(2)	(8^+)	1104.1(2)	6.1(5)

energy. By using the intensity of the $2^+\rightarrow0^+$ transition (see Table I), the intensity of the mass-separated ^{100}In beam was determined to be approximately 2 atoms/s at an average primary ^{58}Ni beam intensity of 43 particle nA.

C. Total-absorption experiment

The total-absorption spectrometer, which is described in detail in Ref. [22], consists of a large NaI crystal of 356 mm diameter and 356 mm length and is equipped with ancillary detectors for registering β particles, protons, and x rays, as illustrated in Fig. 1. Two silicon (Si) detectors of 450 μm thickness were mounted above and below the source position. They are in the following referred to as "top" and "bottom." The bottom detector, viewing the tape from the side where the ions were implanted, was used to detect positrons and protons. The top detector, placed at the opposite side of the tape, served to record positrons and thus to identify βp
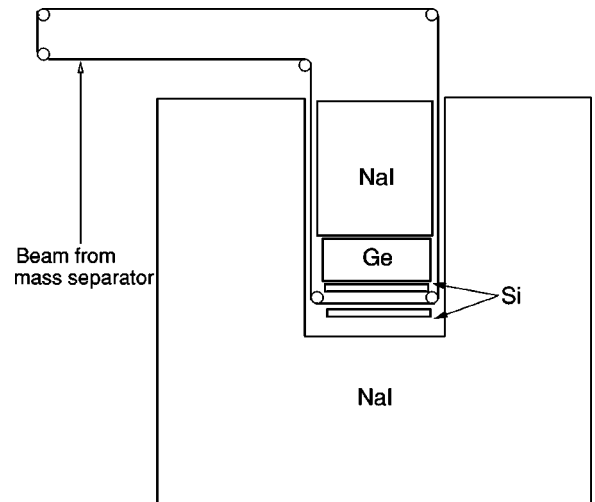

FIG. 1. Schematic drawing of the TAS equipped with ancillary Si and Ge detectors. See text for details.

events by a top-bottom coincidence. An energy deposition in the bottom detector above 1.5 MeV was assigned to the detection of a β-delayed proton event, whereas energies lower than 1.5 MeV were considered to be due to a positron detection. A small contamination from registration of positrons in the "proton gate" was taken into account by extrapolating the low-energy spectrum recorded in the bottom Si detector to higher energies. A Ge detector of 10 mm thickness for x-ray spectroscopy was placed above the top Si detector [22]. By requiring coincidences between the Ge detector and the TAS, we selected the electron capture (EC) component of the β decay. The Ge detector allowed us to inspect contaminants of the implanted sources.

In contrast to the high-resolution measurement, a special technique for suppressing the isobar contamination of cadmium and silver isotopes is mandatory due to the low resolution of the TAS. The release of ^{100}In from the ion source was temporarily separated from that of ^{100}Cd and ^{100}Ag by an alternately heated and cooled pocket [23].

The mass-separated $A=100$ beam was implanted in a transport tape which, in stepwise operation, moved the activity to the center of the TAS where it came to rest in the position between the Si counters. A period of 16 s for the implantation-measurement cycle was chosen. After four consecutive implantations of TAS sources, the beam was directed for one collection interval to a separate tape collector, where a standard Ge detector was used to monitor the beam purity, while TAS registered background radiation. The total measurement time amounted to 20 000 cycles, corresponding to 90 h. The intensity of the mass-separated ^{100}In beam was estimated on the basis of the TAS data to be about 1.6 atoms/s.

III. RESULTS OF THE HIGH-RESOLUTION MEASUREMENT

A. Energy spectra of γ rays measured in coincidence with positrons

Figure 2 displays the sum spectrum obtained by sorting the individual signals from all Ge crystals registered in coincidence with positrons. The strongest transitions assigned to the ^{100}In decay are the peaks at 297, 795, and 1004 keV, followed by the less intense 363-, 453-, 658-, and 1042-keV lines. New γ rays of 1068, 1104, 1365, and 1513 keV have been assigned to the ^{100}In decay. Apart from these transitions, a sizable amount of the isobaric contaminant ^{100}Ag, and therefore transitions occuring in the daughter ^{100}Pd, were identified in the spectrum. The 451/453-keV doublet, containing γ transitions in ^{100}Pd and ^{100}Cd, was partially resolved. Random coincidences with gamma rays from the room background are also present in the spectrum. The experimental energies and intensities of β-delayed γ rays of ^{100}In observed in this work are presented in Table I.

B. Determination of the ^{100}In half-life

In order to obtain information concerning the half-life of ^{100}In, the time distribution of the intensities of β-delayed γ rays was sorted and analyzed. For each of the three strongest
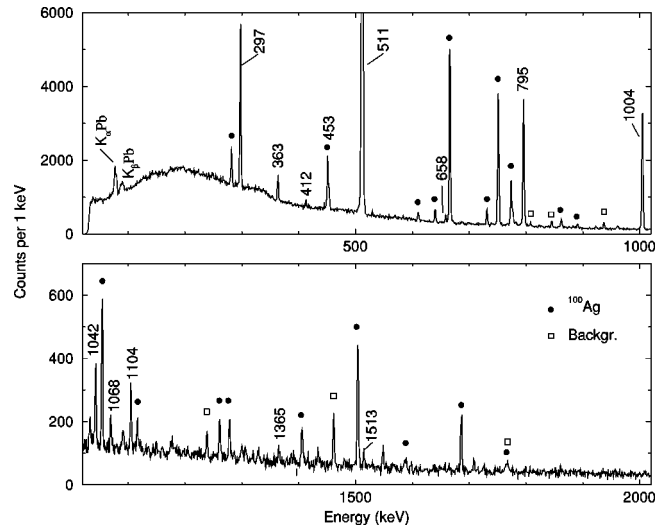

FIG. 2. Gamma-ray spectrum obtained at mass $A=100$ in coincidence with positrons. Excepting the 511-keV annihilation peak, the lines labeled with their energies in keV were identified as β-delayed γ rays of ^{100}In. The lines marked by symbols are transitions from the isobaric-contaminant decay ^{100}Ag$\rightarrow^{100}$Pd or from the room background.

lines a fit of the grow-in curve with one exponential function was performed, as illustrated in Fig. 3. The results are listed in the first three lines of Table II. The average half-life based on high-resolution data agrees with the values deduced from TAS(β^+), TAS(EC), and βp data obtained in the present work (see Secs. IV A and IV C and Table II).

C. ^{100}In$\rightarrow^{100}$Cd β-decay scheme

Events containing $\beta\gamma\gamma$ coincidences were recorded on tape and sorted off-line into two-dimensional matrices. The $\gamma\gamma$ coincidences were analyzed in the positron-gated matrix
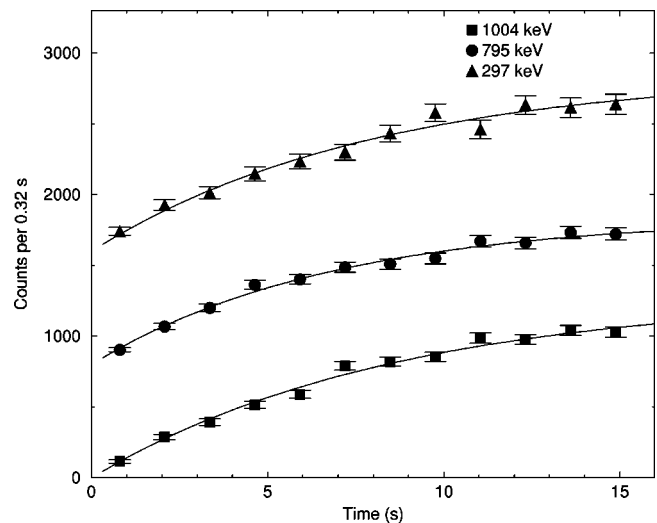

FIG. 3. Time dependence of the 1004-, 795-, and 297-keV transitions. To avoid overlap of the data points, the intensities of the 795- and 297-keV γ rays were shifted by 800 and 1600 counts, respectively.

TABLE II. Half-life of ^{100}In determined in the high-resolution and the TAS measurements. The weighted half-life is built from the listed individual values.

Spectrum condition		$T_{1/2}$ (s)
γ rays	297 keV	5.4(7)
γ rays	795 keV	4.8(4)
γ rays	1004 keV	6.2(4)
TAS	γ_{TAS} and β^+, $E_{TAS} \geq 7$ MeV	6.1(2)
TAS	γ_{TAS} and X(Cd), $E_{TAS} \geq 5$ MeV	5.5(7)
Protons	$E_p \geq 2$ MeV	6.8(8)
		$\bar{T}_{1/2} = 5.9(2)$

by using the RADWARE program [24]. Examples of background corrected β-gated γ-ray spectra, obtained in coincidence with the 1004- and 795-keV γ rays, are displayed in Fig. 4. In the upper panel, strong coincident transitions at 297 and 795 keV appear, thus defining the main deexciting sequence. The 453-keV transition deexciting the 8^+, 2549-keV isomer [6], is also seen in the spectrum. This observation is due to the fact that the half-life of 60(3) ns of this isomeric level is short compared to the coincidence time window of 8 μs (see Sec. II B). Peaks at 1042 and 412 keV are also visible in the 1004-keV gate, but not in the 795-keV gate (see lower panel of Fig. 4). In both spectra, weak coincidences at 1068 and 1365 keV can be seen, their intensities amounting approximately to 2% and 3% of that of the 1004-keV γ ray, respectively (see Table I). Moreover, the 1068-keV transition is in coincidence with the 297- and 795-keV γ rays, while the 1365-keV line is observed in coincidence with the latter transition only. Thus a hitherto unobserved ^{100}Cd level at 3164 keV excitation energy has been firmly established. In addition, in the 1004-, 795-, and 297-keV gates a new transition at 1104 keV was observed.

Based on the $\beta\gamma\gamma$ coincidence data, the ^{100}In$\rightarrow^{100}$Cd decay scheme is presented in Fig. 5. It comprises two new
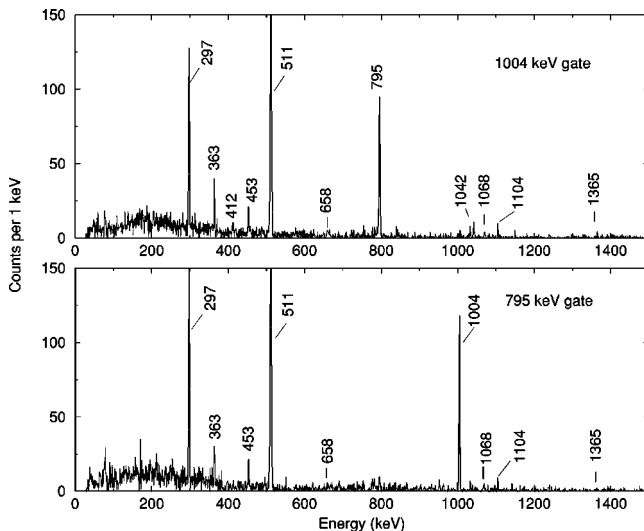

FIG. 4. Coincidence spectra gated on the 1004- and 795-keV transitions, respectively, obtained from the $\beta\gamma\gamma$ matrix. Transitions in ^{100}Cd are marked by their energies in keV.
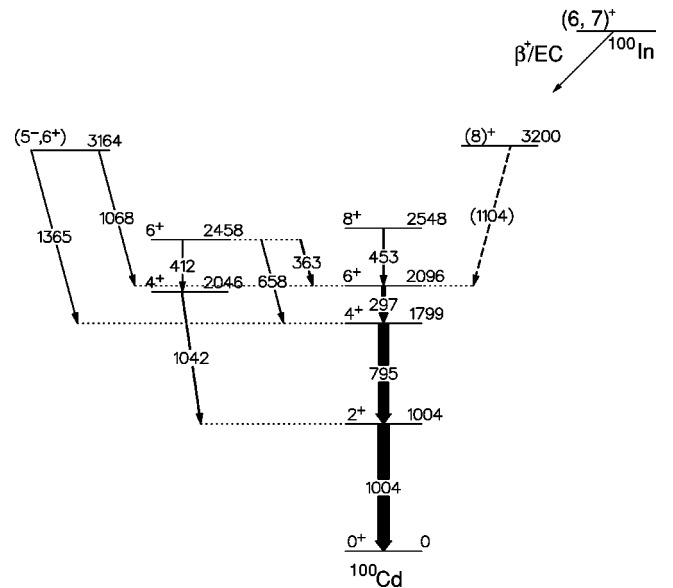

FIG. 5. ^{100}In $\rightarrow$ ^{100}Cd decay scheme obtained by analyzing $\beta\gamma\gamma$ coincidences.

nonyrast ^{100}Cd levels and three new γ rays compared to the data obtained previously in in-beam experiments [6–8]. We confirm the main $E2$ sequence deexciting the 8^+ isomer to the ground state, and also the yrare 6^+ and 4^+ levels at 2458 and 2046 keV, respectively, and their subsequent decay. The spin and parity assignments of the 3164-keV level will be discussed in the shell-model section, see Sec. V. The 1104-keV transition was tentatively placed as deexciting the new 3200-keV level (see Fig. 5). Due to weak and ambiguous coincidence relations between the known transitions and the newly observed 1513-keV γ ray, the latter could not be placed in the level scheme. The spin and parity assignments of the β-decaying ^{100}In state and of ^{100}Cd levels will be further discussed in Secs. IV C and V.

The "apparent feeding" ($I_{\beta\gamma}$), that one may determine by performing the γ-ray intensity balance on the level scheme shown in Fig. 5, is related to direct β feeding (I_β) *and* to unobserved γ feeding following the β decay to higher-lying levels (I_γ^{high}). This is the reason why it is not straightforward to get an insight into the I_β values by inspecting the $I_{\beta\gamma}$ data (see also Ref. [25]). This topic will be further discussed in Secs. IV B, IV C, and V C.

IV. RESULTS OF THE TAS MEASUREMENT

A. TAS spectra

Despite of the strong suppression of the ^{100}Ag activity, it still dominated the implanted $A=100$ samples. For the EC mode this is reflected in the x-ray spectrum which is presented in Fig. 6(a). The strongest peaks are those corresponding to Pd x rays following the ^{100}Ag decay. The Ag x-ray peak is due to the decay of ^{100}Cd, which was accumulated as a ^{100}In daughter, while Cd x rays originate from ^{100}In decay.

The absorbed energies in the TAS(β^+) spectrum exceed the level energies by 1022 keV, due to the summation of γ cascades with positron annihilation quanta. It is expected that
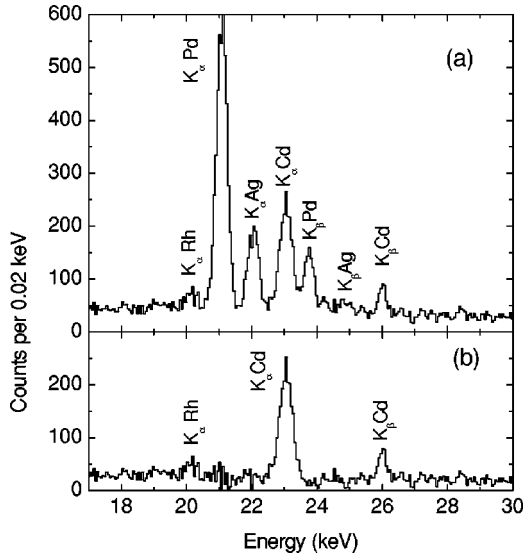
FIG. 6. X-ray spectra registered by the small Ge detector inside TAS before (a) and after (b) contaminant subtraction. Peaks assigned to the decays of ^{100}Ag, ^{100}Cd, and ^{100}In, i.e., Pd, Ag, and Cd x rays, respectively, are accordingly labeled. Traces of Pd were detected on tape and therefore Rh x rays are present in (a) and (b).
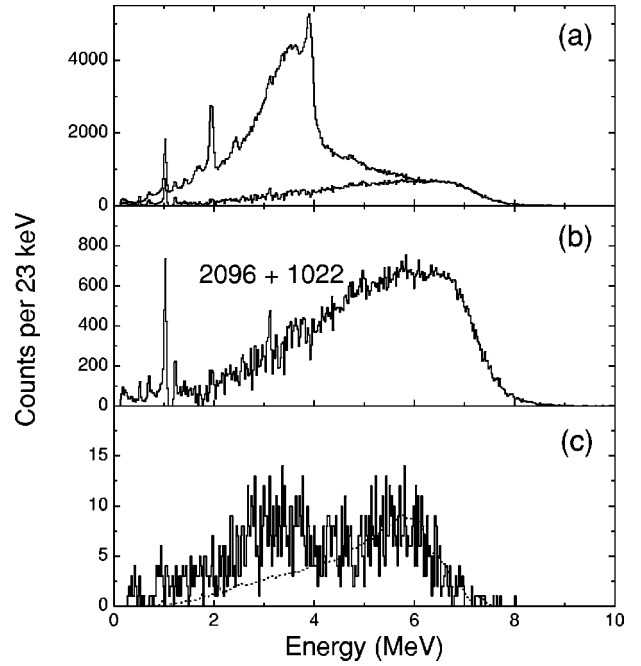

FIG. 7. Experimental TAS spectra obtained in coincidence with positrons registered in the Si detectors, (a) and (b), and Cd x rays (c). Panel (a) presents the TAS(β^+) data with and without contaminant subtraction, panel (b) shows the corrected spectrum once again on an expanded scale. The strong line at 1 MeV in (b) is due to a contaminant present on the tape. The peak at about 3 MeV in the TAS(β^+) spectrum, corresponding to the 2.096-MeV level, is due to direct γ feeding following β decay (see text). In panel (c), the simulated spectrum is presented as dashed line (see Sec. IV C).

the TAS(β^+) spectrum is free of contaminants for absorbed energies above 7 MeV, i.e., the upper limit corresponding to the largest Q_{EC} value amongst the isobaric contaminants [7.05(8) MeV of ^{100}Ag [26]]. A half-life of 6.1(2) s was found for the TAS(β^+) spectrum at absorbed energies larger than 7 MeV, in agreement with the value of 6.2(4) s obtained from the most intense γ ray observed in the high-resolution measurement (see Table II). However, at lower energies the isobaric contamination is detrimental for the TAS(β^+) spectrum shown in Fig. 7(a), where the pronounced structures are due to ^{100}Ag, ^{100m}Ag, and ^{100}Cd decays. In order to purify the ^{100}In TAS(β^+) spectrum from isobaric contamination, sources abundant in ^{100}Ag, ^{100m}Ag, and ^{100}Cd were prepared and measured in separate experiments. Properly normalized, the corresponding reference spectra were subtracted from those enriched in ^{100}In. A normalization for this procedure was found by demanding complete removal of the x and γ rays from the decay of the isobaric contaminants, as it is shown in Fig. 6(b). Because of the contribution from tails of the Pd and Ag x-ray peaks under the Cd peak, such a procedure was applied not only to the TAS(β^+) spectra, but also to the x-ray gated TAS(EC) spectrum. The TAS(β^+) and TAS(EC) spectra obtained after the subtraction are displayed in Figs. 7(b) and (c). In the TAS(EC) spectrum two different structures are visible. A half-life of 5.5(7) s (see Table II) was obtained for events with absorbed energies higher than 5 MeV, whereas the low-energy part, including the pronounced excess of counts in the region below 4 MeV, is characterized by a considerably longer half-life of 14(4) s. The long-lived events in the TAS(EC) spectrum cannot be removed by a reasonable renormalization of the isobaric contaminants. Excluding the value of 14 s, the weighted average of the half-life of ^{100}In obtained in this work is 5.9(2) s (see Table II). This result is in agreement with, but more accurate than, the

previous values of 6.1(9) s [12] and of 6.6(7) s [14].

The observation of two time components in the TAS(EC) spectrum might be due to a long-lived isomer in ^{100}In or ^{100}Cd. However, the lack of statistics does not allow us to clarify this issue. Therefore we refrain from interpreting the low-energy structures of the TAS(EC) spectrum and restrict the following discussion to its short-lived high-energy part.

B. Beta intensity

The ^{100}Cd levels identified in the high-resolution measurement should be observed as peaks in the net TAS(β^+) spectrum shown in Fig. 7(a), provided that they are directly populated by sizable β or γ feeding. However, the spectrum is rather unstructured, except for one peak that can be reliably distinguished from statistical fluctuations. It occurs at an absorbed energy of 3120 keV, as presented in Fig. 7(b), and is assigned to the feeding of the 6^+ level, observed in the high-resolution experiment at 2096 keV (see Fig. 5).

In the following, the area of such a peak in the TAS spectrum and its composition from direct β and γ feeding following β decay will be discussed. The area S of the resolved peak can be written as

$$S = \epsilon_{fa}[I_\beta + \Sigma(1-\epsilon_{tot})I_\gamma^{high}], \qquad (1)$$

where ϵ_{fa} is the efficiency of the full absorption of the γ cascade deexciting the level, I_β and I_γ^{high} are parameters de-

fined in Sec. III C, and the sum runs over all levels which are directly β populated and deexcite by emitting one γ ray, and ϵ_{tot} is the efficiency for detecting this γ transition. The probability for a γ ray to escape from detection is $(1-\epsilon_{tot})$, and the value ranges from 0.05 to 0.2, depending on its energy. This factor is of crucial importance whenever strong β feeding occurs in the high-energy region. Therefore to decide if a pronounced peak is directly populated by β feeding or is rather a result of an incomplete γ detection, a calculation of the I_β is mandatory. In the following, we use the notation I_β for both β feeding to resolved levels and for the quasicontinuum β-feeding distribution in the high-energy region as only levels relevant for the GT transition are regarded.

The procedure of deriving I_β values from the experimental TAS spectra was described in detail in Refs. [10,27]. The observed TAS(β^+) and TAS(EC) spectra represent convolutions of the respective β^+ and EC intensity distributions with the response function of the spectrometer. We used the decay scheme established from the high-resolution experiment as a basis for constructing the TAS response matrix. For the γ cascades from the experimental low-lying levels, the γ branching ratios according to the decay scheme were used. The γ cascades from the high excitation energies were simulated by using a statistical analysis. Expressions for the γ-ray strength functions were taken from literature for $E1$ [28], $M1$ [29], and $E2$ [30]. In contrast to the usual practice, we replaced the statistical level density by the levels obtained from shell-model calculations by using the code OXBASH (for details see Sec. V). The γ-branching ratios to the experimentally established levels were adjusted to reproduce the γ-ray intensity presented in Table I and Fig. 5. The use of the shell-model level predictions as input for the iteration process enables a consistent description of the statistical simulation in the whole excitation-energy region, as only levels relevant for the GT transition are regarded.

In order to extract the I_β distribution, the experimental TAS(β^+) and TAS(EC) spectra were fitted by simulated spectra varying the I_β distribution. The TAS(β^+) spectrum was fitted for absorbed energies up to 10 MeV. Since only the high-energy part of the TAS(EC) spectrum can be reliably assigned to the ^{100}In decay, the fit of this spectrum was restricted to absorbed energies above 5 MeV. The simultaneous fit of the TAS(β^+) and TAS(EC) spectra implies that the Q_{EC} value of ^{100}In is adjusted during the least-squares procedure. Due to the lack of statistics, only a rough estimate of 10.0(5) MeV was obtained for this quantity. A more precise Q_{EC} evaluation will be discussed in Sec. IV C. The simulated TAS(EC) spectrum is shown in Fig. 7(c) as well.

Figure 8(a) presents the I_β distribution and Table III shows the I_β values of individual ^{100}Cd levels in bins of 200 keV width. The main part of the I_β distribution is characterized by a resonance occurring at excitation energies above 4 MeV, peaking at 6.2 MeV and having a full width at half maximum (FWHM) value of about 1 MeV. The small scale fluctuations of the I_β distribution at low energies which can be seen from Fig. 8(a) are comparable to the statistical uncertainties.
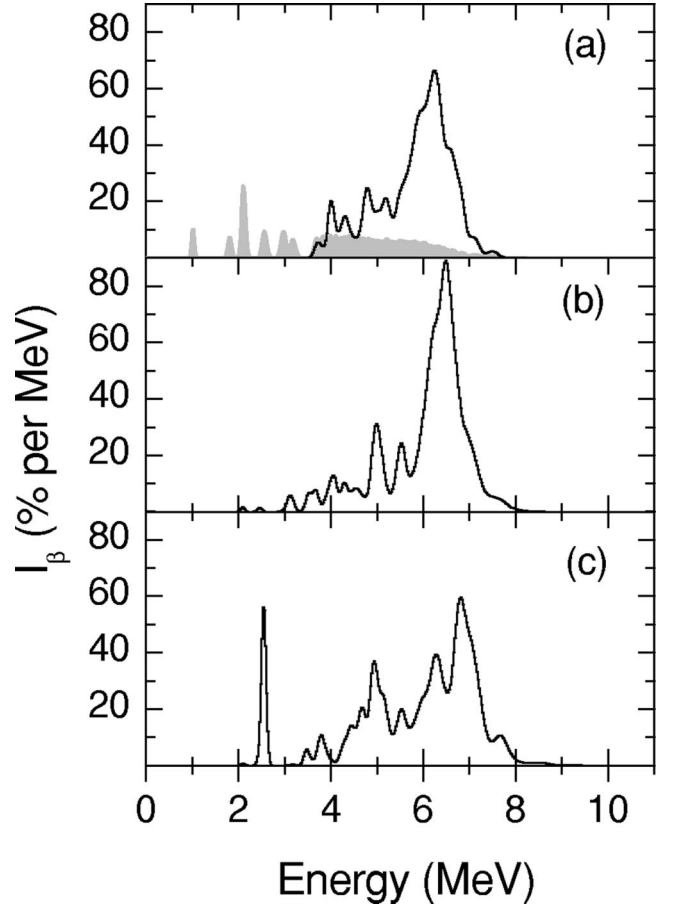

FIG. 8. Beta-intensity distribution deduced from the TAS experiment (a), and from the shell-model predictions (model A), under hypotheses of a 6^+ (b) and 7^+ (c) assignment for the ground state of ^{100}In. The experimental uncertainties are indicated as a shadowed area in panel (a). The calculations have been folded with a Gaussian function having a width equal to the experimental TAS resolution.

TABLE III. Beta feeding (I_β) and β-delayed proton intensities ($I_{\beta p}$) of the decay of ^{100}In to high-lying ^{100}Cd states. The data are given for 0.2-MeV intervals of the ^{100}Cd excitation energy.

Interval (MeV)	I_β(%)	$I_{\beta p}$(%)	Interval (MeV)	I_β(%)	$I_{\beta p}$(%)
3.6	0.93		6.2	13.50	0.04
3.8	2.11		6.4	9.01	0.05
4.0	3.00		6.6	7.09	0.03
4.2	2.89		6.8	3.41	0.16
4.4	1.77		7.0	1.50	0.22
4.6	3.86		7.2	0.53	0.20
4.8	4.21		7.4	0.46	0.28
5.0	4.06		7.6	0.13	0.18
5.2	3.68		7.8		0.13
5.4	5.05		8.0		0.09
5.6	4.48		8.2		0.06
5.8	10.90		8.4		0.05
6.0	12.70		Total	98.4	1.6

TABLE IV. Experimental and theoretical data on excited ^{100}Cd levels. Level energies (E_x), spin and parities (J^π), experimental apparent feeding ($I_{\beta\gamma}$), shell-model γ feeding following the β decay to higher-lying levels (I_γ^{high}), and experimental and shell-model β feeding (I_β). The experimental $I_{\beta\gamma}$ values, obtained by performing the γ-ray intensity balance of the decay scheme, include both β population of a given level and the I_γ^{high} feeding. The model results stem from the latter process only. The theoretical intensities are predicted by model A assuming spins of 6^+ (SM_{6^+}) or 7^+ (SM_{7^+}) for the β-decaying ^{100}In state.

E_x	J^π	$I_{\beta\gamma}$	I_γ^{high}		I_β		
(keV)	($\hbar$)	EX(%)	SM_{6^+}(%)	SM_{7^+}(%)	EX(%)	SM_{6^+}(%)	SM_{7^+}(%)
1004	2^+	5(7)			<1.0		
1799	4^+	21(8)	8.4	1.6	<0.9		
2046	4^+	5.3(7)	6.3	1.2	<0.9		
2096	6^+	33(3)	25.5	21.8	<3.0	0.18	0.07
2458	6^+	16(1)	16.2	13.9	<1.3	0.19	0.32
2549	8^+	9.4(8)	7.6	19.0	<1.3		7.14
3164	(6^+)	5.4(6)	6.0	5.2	<1.8	0.50	0.04
	(5^-)		7.7	4.5			
3200	(8^+)	6.1(5)	3.0	7.5	<1.8		0.005

For all levels established in the high-resolution experiment (see Table I), including the 2096-keV level which was the only pronounced peak in the TAS(β^+) spectrum, as observed in Fig. 7(b), we only obtain upper limits for I_β. These values are presented in Table IV. The total β^+ feeding to all these levels is less than 12%. The simulation has shown that the 2096-keV peak is mainly due to γ feeding following β decay. It is worth noting that a similar conclusion has been drawn from a TAS study of ^{104}In β decay where, despite much better counting statistics, the TAS spectra did not show any pronounced peaks in the low-energy region [31]. The interpretation of these results in connection with high-resolution data and with shell-model calculations will be given in Secs. V B and V C.

C. Beta-delayed proton emission

The low-energy part of the proton spectrum registered by the bottom Si detector contains a sizable contribution of positron events, see Fig. 9(a). In order to clarify this effect, we used the two-dimensional TAS-Si matrix and inspected it for different thresholds of the bottom Si and TAS detectors. If we require coincidences between the bottom Si detector and TAS energies, $E_{TAS} < 1.1$ MeV, the positron contamination is suppressed and mainly βp events are selected. This is illustrated in Fig. 9(b). Figure 9(c) shows the spectrum of β-delayed protons that follow the EC decay of ^{100}In and populate the ^{99}Ag ground state. In order to select these events, an anticoincidence with TAS signals was required. A half-life of $T_{1/2} = 6.8(8)$ s was measured for βp events with $E_p \geq 2$ MeV (see Table II), in agreement with the value deduced from the high-resolution data.

1. ^{99}Ag levels fed by β-delayed protons

Figure 10 displays the TAS spectrum obtained in coincidence with protons registered in the bottom Si detector, selected under the condition that $E_{bottom} \geq 1.5$ MeV. In order to estimate the contribution from positrons, a normalized

TAS(β^+) spectrum is shown in the same figure. It is seen that for the energy window discussed above, the contribution of the high-energy positron tail is negligible. One can see in the figure that the TAS spectrum following the delayed protons is located within an energy window of $E_{TAS} \leq 1.1$ MeV, which corresponds to the TAS gate used in the previous section.
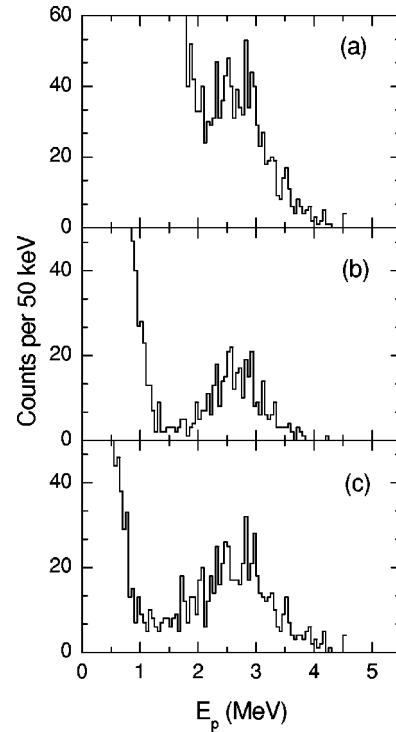

FIG. 9. Proton spectrum obtained in the bottom Si detector without TAS selection (a), in coincidence with TAS energies ≤ 1.1 MeV (b), and in anticoincidence with TAS (c). The latter condition selects the EC-delayed protons which are emitted to the ^{99}Ag ground state.
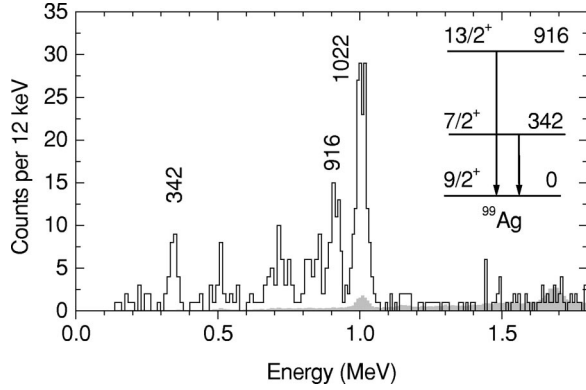
FIG. 10. TAS spectrum obtained in coincidence with protons registered in the bottom Si detector. The contribution due to the estimated positron background in the proton gate is shown in the shadowed area. In the inset, the lowest excited states in ^{99}Ag which are fed by delayed-proton emission are shown.

In the spectrum, apart from the annihilation peak, which corresponds to the βp emission to the ^{99}Ag ground state, there are two more peaks which can be unambiguously assigned to known levels in ^{99}Ag. These are the $7/2^+$ state at 342 keV known from β-decay studies [32], and the $13/2^+$ state at 916 keV assigned by in-beam work [33]. Since the annihilation peak dominates the spectrum, it is evident that the main fraction of the βp related intensity goes to the $9/2^+$ ground state of ^{99}Ag. Table V lists the partial intensities of the proton emission to states in ^{99}Ag. The intensity is normalized to 100 βp events. The uncertainties are mainly due to the extrapolation of the background in the proton spectra. The total branching ratio for βp emission following the ^{100}In decay was found to be 1.6(3)%.

The relative βp emission feeding levels of different spins in ^{99}Ag is sensitive to the spin value of the β-decaying ^{100}In state. Hence an analysis of experimentally measured feeding may provide information about the ground-state spin and parity of ^{100}In. On the basis of the statistical approach discussed in Ref. [34], and of the total experimental energy distribution of EC-delayed protons (ECp), we calculated the relative intensities of the ECp emission to ^{99}Ag states, assuming spin and parity values of 5^+, 6^+, 7^+, and 8^+, for the ^{100}In ground state. Table VI presents the comparison between the experimental and calculated βp intensities. The agreement between the experimental values and the calculation is definitely better under the assumptions that the ground state of ^{100}In has spin and parity of 6^+ or 7^+, while the other assumptions of spins of 5 and 8 can be rejected. However, the differences between the competing two spin-parity hypotheses are not significant enough to allow one to draw a definite conclusion.

TABLE V. Experimental intensities of the βp and ECp emission to the ^{99}Ag states.

	$9/2^+$	$7/2^+$	$13/2^+$
$I_{\beta p}(\beta^+)(\%)$	60(6)	2.8(5)	6.2(12)
$I_{\beta p}(EC)(\%)$	31(5)	$\leqslant 1$	$\leqslant 2$

TABLE VI. Comparison of calculated and experimental ECp intensities for the lowest-lying $9/2^+$, $7/2^+$, and $13/2^+$ ^{99}Ag states.

^{100}In	^{99}Ag states		
Ground state	$9/2^+$	$7/2^+$	$13/2^+$
5^+	720	120	22
6^+	610	51	50
7^+	320	28	70
8^+	180	4.4	76
EXP	570(60)	27(5)	62(12)

2. Determination of the Q_{EC} value of ^{100}In

By using the energy distribution $[I_{\beta p}(EC)]$ of the ECp events, and the total intensity ΣI_β of βp emission fed to the ^{99}Ag ground state, we estimated the $Q_{EC}-S_p$ value of ^{100}In decay to be 5.25(13) MeV, where S_p is the proton-separation energy of ^{100}Cd. The $Q_{EC}-S_p$ value was found by using the condition
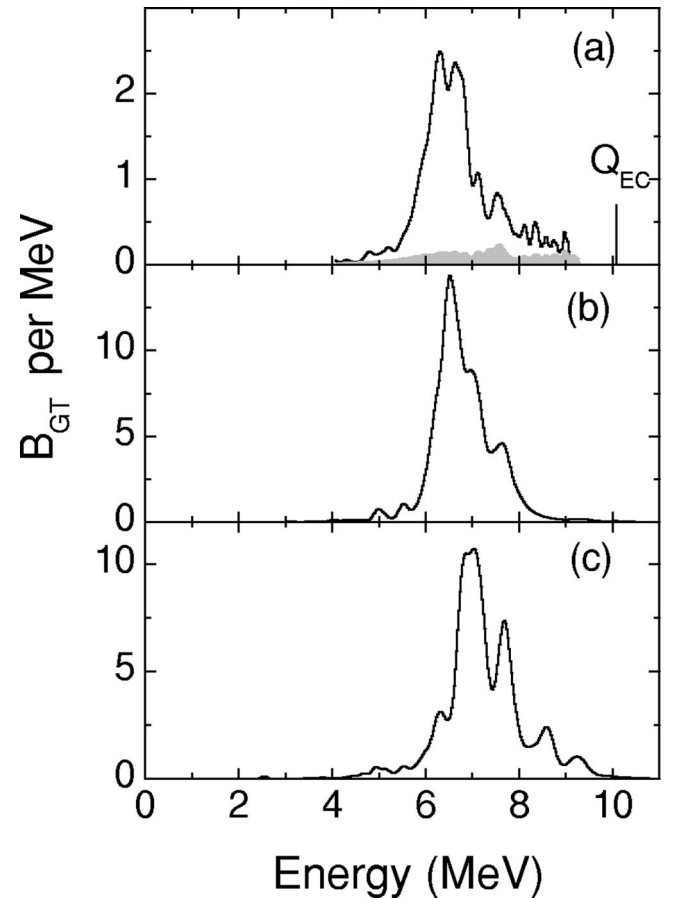

FIG. 11. Total experimental B_{GT} distribution (a) compared to theoretical distributions calculated in shell model A for parent spin-parity assumptions of 6^+ (b) and 7^+ (c). The experimental Q_{EC} value is indicated by a vertical line. The experimental uncertainties are indicated as a shadowed area in panel (a). Above 6.3-MeV energy proton contributions can be seen in panel (a).

$$\sum I_{\beta p} = \sum I_{EC} f_{\beta^+} / f_{EC}, \qquad (2)$$

where f_{β^+} and f_{EC} are the statistical Fermi functions for β^+ and EC transitions, whose ratio is a function of the β-decay energy. Using an S_p value of 4.83(19) MeV [26], a Q_{EC} value of 10.08(23) MeV is obtained. The Q_{EC} uncertainty takes into account the uncertainty related to the delayed protons of 0.13 MeV and that of the S_p value of 0.19 MeV. The Q_{EC} value should be compared to the experimental value of 9.5(4) MeV obtained in Ref. [35] by mass measurements, to the evaluated value of 10.18(30) MeV from Ref. [26], and to a shell-model prediction of 10.07 MeV [36].

D. The experimental B_{GT} distribution

The GT distribution as calculated from the I_β distribution by standard procedures [27], making use of the Q_{EC} value of 10.08(23) MeV adopted in Sec. IV C, and using the ^{100}In half-life of 5.9(2) s discussed in Sec. IV A, is shown in Fig. 11(a). The centroid of the GT resonance is located at an excitation energy of 6.4 MeV and has a width of approximately 1 MeV. The partial strength detected by the TAS in γ rays is determined to be $B_{GT,\gamma} = 3.0(9)$. The B_{GT} is given in units of $g_A^2/4\pi$. The uncertainty includes that of the I_β distribution of 0.60, and that of the Q_{EC} value originating from the S_p value of 0.70, the latter being the dominating contribution. This implies that the latter value ought to be measured with higher precision. Similarly, the delayed proton branch results in a partial GT strength of $B_{GT,p} = 0.86(15)$. The $B_{GT,p}$ uncertainty originates from the βp counting statistics and the half-life determination, and contains a minor contribution from the $Q_{EC} - S_p$ value. The total GT strength is $B_{GT,\gamma} + B_{GT,p} = 3.9(9)$. The comparison of the experimental B_{GT} distribution to the theoretical predictions will be made in Sec. V B.

V. SHELL-MODEL CALCULATIONS AND DISCUSSION

To gain insight into the microscopic structure of states in ^{100}Cd and ^{100}In, and to study the GT resonance in ^{100}In $\rightarrow$ ^{100}Cd β decay, shell-model calculations were performed using the code OXBASH [37]. The model space for the valence protons comprises the $0g_{9/2}$ and $1p_{1/2}$ orbitals, while the neutron single-particle orbitals are $1d_{5/2}$, $0g_{7/2}$, $2s_{1/2}$, $1d_{3/2}$, and $0h_{11/2}$. The single-particle energies relative to a ^{88}Sr core were chosen to reproduce the extrapolated values for a ^{100}Sn core [38], namely $\epsilon^\pi_{0g_{9/2}} = -2.92$ MeV, $\epsilon^\pi_{1p_{1/2}} = -3.53$ MeV, $\epsilon^\nu_{1d_{5/2}} = -11.15$ MeV, $\epsilon_{0g_{7/2}} = -11.07$ MeV, $\epsilon^\nu_{2s_{1/2}} = -9.60$ MeV, $\epsilon^\nu_{1d_{3/2}} = -9.50$ MeV, and $\epsilon^\nu_{0h_{11/2}} = -8.60$ MeV.

The effective interaction was derived by employing a perturbative many-body scheme starting from the free nucleon-nucleon interaction, according to the prescription outlined in Ref. [39]. For calculating the GT-strength distributions the free GT operator was used. We refer to this approach as model A. The model results are presented in Figs. 8, 11, 12, and 13 in comparison with the experimental data.
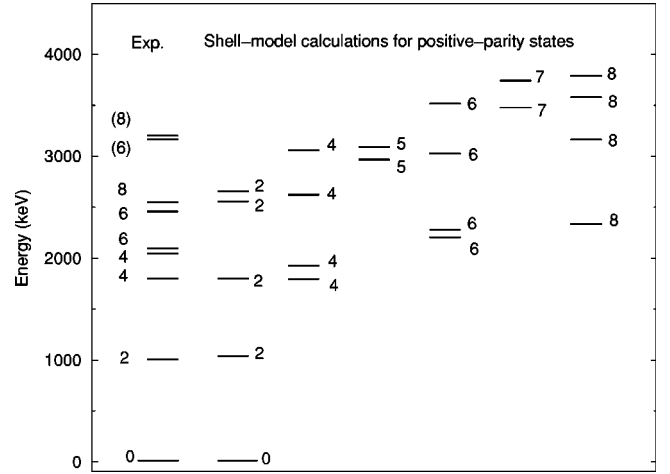

FIG. 12. Comparison of experimental ^{100}Cd level energies with shell-model predictions from model A. In the first column the experimental energy levels are presented. The other columns comprise yrast and yrare groups of theoretical states ordered according to their spin and energy.

Alternatively, in Ref. [36] the role of np-nh excitations ($n=0$–2) of the ^{100}Sn core was studied in a model space consisting of $0g_{9/2}$, $1p_{1/2}$, $1d_{5/2}$, $0g_{7/2}$, $2s_{1/2}$, and $1d_{3/2}$ orbitals for both protons and neutrons. The theoretical levels in ^{100}In and ^{100}Cd were calculated in the JS4 and JS6 approaches, respectively. The corresponding ^{100}In$\rightarrow$^{100}Cd β-strength distribution was deduced. We will refer to this as model B. Finally, the total GT strength for the ^{100}In $\rightarrow$^{100}Cd decay was calculated in the model space A [31] using the approach of Ref. [5] and the modified interaction as described in Ref. [27].

A. ^{100}Cd low-lying states

In this section the results obtained by using model A and shown in Fig. 12 are discussed. For all the shell-model states
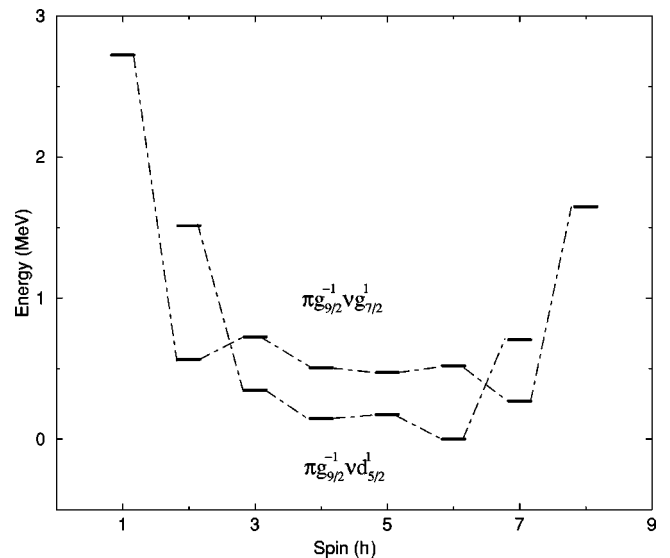

FIG. 13. Calculated level energies of the $\pi g_{9/2}^{-1} \nu g_{7/2}$ and $\pi g_{9/2}^{-1} \nu d_{5/2}$ multiplets of ^{100}In by using model A. States belonging to the same multiplet are connected to guide the eye.

presented in Fig. 12, the proton contribution to the wave function is largely dominated by two holes in the $g_{9/2}$ and two particles in the $p_{1/2}$ orbitals, the other configurations with different occupancies playing no significant role. In the following, the structure of the states with respect to the neutron contributions will be discussed. The first excited state with $J^\pi = 2^+$ is very close to the experimental value. It has a mixed configuration, where both valence neutrons occupy mainly the $1d_{5/2}$ orbital (47%), while about 20% of the amplitude comes from the $0g_{7/2}$ orbital. The 4_1^+ state, correctly predicted in energy, has the same dominant structure as the 2_1^+ state, which remains valid for the 6_1^+ state as well. The 4_2^+ wave function is more fragmented since the dominant configuration is identical to that of 4_1^+ state, but significant contributions originate from neutrons either in $d_{5/2}^1 d_{3/2}^1$ or in $g_{7/2}^1 d_{5/2}^1$ multiplets. This is the lowest state where the pair of valence neutrons is distributed over two subshells; the next state of this character is 6_2^+. The different wave functions of the 4_1^+ and 4_2^+ states result in a lower mixing between the corresponding levels which leads to two close-lying 4^+ states, in agreement with the experiment. A more dramatic effect is observed for the first two 6^+ states, since their wave functions have no major overlap, and thus their energy spacing is calculated to be 78 keV only. In the experiment, this spacing is much larger, which may indicate that the wave functions have a slightly different structure than predicted. The calculated 8_1^+ state, predominantly of $\pi g_{9/2}^{-2}$ character, lies somewhat lower than observed in the experiment. The configuration assignment agrees also with previous shell-model calculations for ^{100}Cd [6], performed in the same model space but using a different set of two-body matrix elements [2,40].

The newly identified experimental level at 3164 keV, with a tentative spin and parity assignment of (6^+), is very close to the calculated 6_3^+ state. The wave function is dominated by a 62% $\nu d_{5/2}^2$ configuration. This is well supported by the experimentally observed decay mode of this level, which feeds the 6_1^+ and 4_1^+ levels, see Fig. 5. The spin and parity assignment for the ^{100}Cd 8_2^+ state at 3200 keV was inferred from a comparison with the shell-model calculations. The structure of the 8_2^+ state is interpreted as having one neutron pair broken and distributed in the $g_{7/2}, d_{5/2}$ orbitals.

B. I_β and GT distributions

The experimental I_β distribution shown in Fig. 8(a) is compared to predictions of model A assuming values of $J^\pi = 6^+$ and of 7^+ for the ^{100}In ground-state spin. The theoretical results are displayed in Figs. 8(b) and (c). Under the assumption that the ground-state spin of ^{100}In is 6^+, the theoretical I_β distribution shows almost no direct feeding (less than 1%) for the 6^+ 2096-keV level, which is close to the experimental finding, as observed in Fig. 7. The centroid position of the resonance is reproduced in the calculations, but not its width. If the ground-state spin is 7^+, a considerable feeding of the 8^+ level is predicted, which is in contra-

diction with the experimental TAS value (see Table IV). The tail of the resonance towards lower energies resembles the experimental one.

The experimental GT distribution is compared in Figs. 11(b) and (c) to shell-model predictions of model A. The distribution from the model A is normalized to a free nucleon GT operator. The position and width of the resonance are reproduced very well. The small upward shift in position can be attributed to the neglect of excitations of the ^{100}Sn core. It has been pointed out earlier [27] that a small renormalization of the proton-neutron interaction strength can account for this shift.

Total GT strengths of 15.9 and 14.4 are calculated for spins of 6^+ and 7^+, respectively, by using the model A. In the approach of Ref. [31] total GT strengths of 15.9 and 15.8 were calculated for spins of 6^+ and 7^+, respectively, whereas 3.9(9) was determined experimentally in the present work. This translates into hindrance factor values of $h = 4.1(9)$ (for 6^+) and of 3.7(9) (for 7^+). These values should be compared to the experimental values of 3.8(7) for ^{98}Cd [5] and to that of 4.3(6) measured for ^{97}Ag [27]. The theoretical hindrance factor of ^{100}Sn is 3.0 [27]. Thus, within the large experimental uncertainties, the ^{100}In β decay exhausts the strength of the GT resonance predicted for ^{100}Sn.

In Sec. IV B the smooth TAS spectrum, the weak feeding of low-lying states (Table IV), and the large β feeding of the GT resonance were discussed. In the light of the shell-model results from the model A the reasons for these results are threefold.

(i) The low-lying ^{100}Cd states of $2qp$ character $\nu d_{5/2} g_{7/2}$ and $\nu g_{7/2}^2$, can be fed by the unpaired $\pi g_{9/2}$ only, whereas the remaining $(\pi g_{9/2})_{0^+}^8$ decay to the GT resonance of $4qp$ states at high excitation energy. As far as β intensities are concerned, the high suppression of the reduced transition rates is largely compensated by the decay-energy selectivity of the f_{β^+} phase-space factor.

(ii) The wave functions of the $J^\pi = 6^+$ to 8^+ ^{100}Cd daughter states as discussed in Sec. V A have little overlap with those of the $4qp$ states. As the two possible parent configurations $(\pi g_{9/2}^{-1} \nu d_{5/2})_{6^+}$ and $(\pi g_{9/2}^{-1} \nu g_{7/2})_{7^+}$ are rather pure (see Sec. V D), the $J^\pi = 6^+$ and 8^+ ^{100}Cd levels cannot be strongly fed in GT decay.

(iii) The dominating $4qp$ GT-resonance configurations $(\pi g_{9/2})_{J_\pi}^8 (\nu d_{5/2} g_{7/2})_{J_\nu}$ and $(\pi g_{9/2})_{J_\pi}^8 (\nu g_{7/2})_{J_\nu}^2$ under the assumption of $J^\pi = 6^+$ or 7^+, respectively, for the ground state of ^{100}In, are connected to the $2qp$ states by strong $M1$ transitions. This can be concluded from the largely different magnetic moments of the $2qp$ and $4qp$ states [6].

C. Beta-delayed γ intensity and spin assignments

For the ^{100}In decay, a strikingly large discrepancy occurs between the $I_{\beta\gamma}$ values deduced from the high-resolution experiment, and the I_β limits inferred from the TAS data (see Table IV). To shed light on this problem, the I_β distribution was calculated by using the model A as a starting point for an estimate of the I_γ^{high} values. A one-step γ decay of the β-fed levels to the experimentally known low-lying levels was as-

sumed. Multipolarities $E1$, $M1$, and $E2$ were considered with strength functions taken from Refs. [28,29,30], respectively. The results are listed in Table IV and represent lower limits due to the restriction to a one-step process. It should be noted that due to the transition energy dependence of the phase-space factor for γ decay, (which is $\sim E_\gamma^n$, where $n = 3$ and 5 for dipole and quadrupole transitions, respectively, in the low-energy limit [41]), the one and two-step processes are greatly favored. Besides the experimental $I_{\beta\gamma}$ and I_β, the calculated values for the assumption of $J^\pi = 6^+$ or 7^+ for the parent state are listed in Table IV. For comparison also the calculated shell-model I_β values are given. The calculations can account for a considerable population of states differing by more than $1\hbar$ from the parent spin under both assumptions, thus proving the aforementioned retention to the common practice in interpreting β-decay data.

A closer inspection of the theoretical results for $I_{\beta\gamma}$, I_β, and I_γ^{high}, and a comparison to the corresponding experimental data, reveal better agreement for the parent spin assumption of $J^\pi = 6^+$. This is demonstrated best for the ^{100}Cd states with $J^\pi = 4^+$, 6^+, and 8^+. The γ feeding of the $J^\pi = 4^+$ states, which for both parent spin options cannot be fed directly in GT β decay, provides a benchmark test for the model input and the validity of the one-step $E1/M1/E2$ assumption. As a consequence, the tentative $J^\pi = (6^+)$ assignment to the state at 3164 keV (see Sec. V A, Table I, and Fig. 5) must be reconsidered. An alternative $J^\pi = (5^-)$ assignment is consistent with the missing intensity, its γ decay and the shell-model prediction of $E_x = 2881$ keV as compared to $E_x = 3027$ keV for the $J^\pi = 6_3^+$ state.

D. ^{100}In ph multiplets

Experimentally, the presented data do not permit us to draw any firm conclusion with respect to the ground-state spin of ^{100}In. The shell-model calculations described as model A were used to make predictions concerning the $\pi g_{9/2}^{-1} \nu d_{5/2}^1$ and $\pi g_{9/2}^{-1} \nu g_{7/2}^1$ multiplet energies in ^{100}In, as displayed in Fig. 13. It is observed that the calculation favors a ground-state spin of 6. The 7^+ state, originating from the $\pi g_{9/2}^{-1} \nu g_{7/2}^1$ multiplet, is located at an excitation energy of 250 keV. Both states have rather pure wave functions with 94% and 70% in the leading configurations for $J^\pi = 6^+$ and 7^+, respectively. The ground state of ^{102}In, being tentatively assigned a spin of 6, originates from the $\pi g_{9/2}^{-1} \nu d_{5/2}^1$ multiplet [11]. Recently, evidence has been presented for a spin-parity assignment of 7^+ [14] to the ground state. At an excitation energy of 145 keV, a state of spin 7 occurs, having a mixed $\pi g_{9/2}^{-1} \nu d_{5/2}^1$ and $\pi g_{9/2}^{-1} \nu g_{7/2}^1$ configuration [11]. In ^{104}In, the lowest members of the $\pi g_{9/2}^{-1} \nu d_{5/2}^1$ multiplet, 6 and 7, respectively, are energetically only 85 keV apart [13]. Based on the aforementioned experimental observations, model A repro-

duces the correct ground-state spin value of $J^\pi = 6^+$ for the heavier indium isotopes. In model B, the ground-state spin and parity for ^{100}In are calculated as $J^\pi = 7^+$, however, at the expense of reversing the $\nu d_{5/2} - \nu g_{7/2}$ order, i.e., placing the $\nu g_{7/2}$ state 230 keV below the $\nu d_{5/2}$ state in ^{101}Sn. This is at variance with recent experimental results from ^{103}Sn [42].

VI. SUMMARY

The decay scheme of ^{100}In, the closest neighbor of ^{100}Sn, was studied in detailed high-resolution and total-absorption spectroscopy. In the high-resolution measurement, $\beta\gamma\gamma$ coincidences allowed us to establish the decay scheme of ^{100}In for the first time and thus to extend the level scheme of ^{100}Cd known from in-beam measurements. The total-absorption results show that ^{100}Cd levels with excitation energies higher than 6 MeV are directly fed by the β^+/EC decay, and a GT resonance is identified at 6.4 MeV. Apparent evidence for β feeding to the identified low-lying states in ^{100}Cd is shown to be mainly due to β-delayed γ feeding. The Q_{EC} value of ^{100}In was determined to be 10.08(23) MeV, in agreement with previous experimental and theoretical estimates. From measurements of the decay curves of γ rays and β-delayed protons, an average ^{100}In half-life of 5.9(2) s was obtained. A purely statistical model analysis of the βp data yielded better agreement with a spin-parity assumption of (6^+) or (7^+) for the ^{100}In ground state, whereas the comparison of the $\beta\gamma$ feeding with predictions based on model A tends to support a (6^+) assignment. Large-scale shell-model calculations using realistic effective interactions and ^{88}Sr as a core yield good agreement with the experimental level energies of ^{100}Cd, and predict a value of 6^+ for spin and parity of the ^{100}In ground state (model A). The GT-distribution properties are well accounted for, implying a GT-hindrance factor as expected for the ^{100}Sn GT decay.

[1] T. Otsuka, R. Fujimoto, Y. Utsuno, B.A. Brown, M. Honma, and T. Mizusaki, Phys. Rev. Lett. **87**, 082502 (2001).

[2] H. Grawe *et al.*, Phys. Scr. **T56**, 71 (1995).

[3] M. Górska *et al.*, *Experimental Nuclear Physics in Europe*, edited by B. Rubio, M. Lozano, and W. Gelletly, AIP Conf. Proc. No. 495 (AIP, Melville, NY, 1999), p. 287.

[4] H. Grawe *et al.*, *Tours Symposium on Nuclear Physics* IV, edited by M. Arnould *et al.*, AIP Conf. Proc. No. 561 (AIP, Melville, NY, 2000), p. 287.

[5] B.A. Brown and K. Rykaczewski, Phys. Rev. C **50**, R2270 (1994).

[6] D. Alber *et al.*, Z. Phys. A **344**, 1 (1992).

[7] M. Górska *et al.*, Z. Phys. A **350**, 181 (1994).

[8] R.M. Clark *et al.*, Phys. Rev. C **61**, 044311 (2000).

[9] K. Rykaczewski *et al.*, Z. Phys. A **322**, 263 (1982).

[10] Z. Hu *et al.*, Phys. Rev. C **62**, 064315 (2000).

[11] M. Lipoglavšek *et al.*, Phys. Rev. C **65**, 021302(R) (2002).

[12] J. Szerypo *et al.*, Nucl. Phys. **A584**, 221 (1995).

[13] D. Seweryniak *et al.*, Nucl. Phys. **A589**, 175 (1995).

[14] A. Stolz *et al.*, *International Nuclear Physics Conference*, edited by E. Norman, L. Schröder, and G. Wozniak, AIP Conf. Proc. No. 610 (AIP, Melville, NY, 2002), p. 728.

[15] R. Barden, R. Kirchner, O. Klepper, A. Plochocki, G.-E. Rathke, E. Roeckl, K. Rykaczewski, D. Schardt, and J. Żylicz, Z. Phys. A **329**, 319 (1988).

[16] C. Mazzocchi *et al.*, in Proceedings of Pingst 2000, Selected Topics of $N = Z$ Nuclei, edited by D. Rudolph and M. Hellström, Lund, Sweden, LUIP003, Bloms i Lund, 2000, p. 29.

[17] E. Roeckl, Nucl. Phys. **A704**, 200 (2002).

[18] R. Kirchner, Nucl. Instrum. Methods Phys. Res. A **292**, 203 (1990).

[19] J. Eberth *et al.*, Nucl. Instrum. Methods Phys. Res. A **369**, 135 (1996).

[20] J. Gerl, K. Vetter, Th.W. Elze, Th. Kröll, and H. Xie, Physics from Large γ-Ray Detector Arrays, Berkeley, LBL 35687, UC413, 1994, p. 159.

[21] K. Schmidt *et al.*, Eur. Phys. J. A **8**, 303 (2000).

[22] M. Karny *et al.*, Nucl. Instrum. Methods Phys. Res. B **126**, 411 (1997).

[23] R. Kirchner, Nucl. Instrum. Methods Phys. Res. B **26**, 204 (1987).

[24] D.C. Radford, Nucl. Instrum. Methods Phys. Res. A **361**, 297 (1995).

[25] J.C. Hardy *et al.*, Phys. Lett. **71B**, 307 (1977); J.C. Hardy, B. Jonson, and P.G. Hansen, *ibid.* **136B**, 331 (1984).

[26] G. Audi, O. Bersillon, J. Blachot, and A.H. Wapstra, Nucl. Phys. **A624**, 1 (1997).

[27] Z. Hu *et al.*, Phys. Rev. C **60**, 024315 (1999).

[28] J.C. Hardy, Phys. Lett. **109B**, 242 (1982).

[29] J. Kopecky and M. Uhl, Phys. Rev. C **41**, 1941 (1990).

[30] M.V. Prestwich and M.A. Islam, Z. Phys. A **315**, 103 (1984).

[31] M. Karny *et al.*, Nucl. Phys. **A690**, 367 (2001).

[32] A.W.B. Kalshoven *et al.*, Nucl. Phys. **A337**, 120 (1980).

[33] W.F. Piel, Jr., C.W. Beausang, D.B. Fossan, R. Ma, E.S. Paul, P.K. Weng, N. Xu, and G. Scharff-Goldhaber, Phys. Rev. C **37**, 1067 (1988).

[34] P. Hornshoj *et al.*, Nucl. Phys. **A187**, 609 (1972).

[35] M. Chartier *et al.*, Phys. Rev. Lett. **77**, 2400 (1996).

[36] I.P. Johnstone and L.D. Skouras, J. Phys. G **21**, L63 (1995).

[37] B.A. Brown, A. Etchegoyen, W.D.M. Rae, N.S. Godevin, W.A. Richter, Ch. Zimmerman, W.E. Ormand, and J.S. Winfried, computer code OXBASH, MSU-NSCL Report No. 524, 1985 (unpublished).

[38] H. Grawe and M. Lewitowicz, Nucl. Phys. **A693**, 116 (2001).

[39] M. Hjorth-Jensen, T.T.S. Kuo, and E. Osnes, Phys. Rep. **261**, 125 (1995).

[40] L.D. Skouras and C. Dedes, Phys. Rev. C **15**, 1873 (1977).

[41] W. Zipper, F. Seiffert, H. Grawe, and P. von Brentano, Nucl. Phys. **A551**, 35 (1993).

[42] C. Fahlander *et al.*, Phys. Rev. C **63**, 021307(R) (2001).